Self-Assembly of Cubes into 2D Hexagonal and Honeycomb Lattices by Hexapolar Capillary Interactions

Giuseppe Soligno,[1] Marjolein Dijkstra,[2] and René van Roij[1]
[1]Institute for Theoretical Physics, Center for Extreme Matter and Emergent Phenomena, Utrecht University, Princetonplein 5, Utrecht 3584 CC, The Netherlands
[2]Soft Condensed Matter, Debye Institute for Nanomaterials Science, Department of Physics and Astronomy, Utrecht University, Princetonplein 5, Utrecht 3584 CC, The Netherlands
(Received 25 April 2016; published 20 June 2016)

Particles adsorbed at a fluid-fluid interface induce capillary deformations that determine their orientations and generate mutual capillary interactions which drive them to assemble into 2D ordered structures. We numerically calculate, by energy minimization, the capillary deformations induced by adsorbed cubes for various Young's contact angles. First, we show that capillarity is crucial not only for quantitative, but also for qualitative predictions of equilibrium configurations of a single cube. For a Young's contact angle close to 90°, we show that a single-adsorbed cube generates a hexapolar interface deformation with three rises and three depressions. Thanks to the threefold symmetry of this hexapole, strongly directional capillary interactions drive the cubes to self-assemble into hexagonal or graphenelike honeycomb lattices. By a simple free-energy model, we predict a density-temperature phase diagram in which both the honeycomb and hexagonal lattice phases are present as stable states.

DOI: 10.1103/PhysRevLett.116.258001

Over a century ago, it had already been observed that submm sized particles strongly adsorb at fluid-fluid interfaces [1,2]. Indeed, a fluid-fluid interface of area A and surface tension γ has a free energy cost γA, and particles can reduce A by adsorbing at the interface. The bonding potential is usually strong enough to allow stable monolayers of particles. Since a pioneering study by Pieranski [3], a lot of interest has been devoted to these quasi-2D systems, which have many applications, e.g., emulsions [4–9], coatings [10,11], optics [12], and new material development [13]. Because of the contact angle constraint imposed by Young's Law, an adsorbed particle in general induces deformations in the shape of the fluid-fluid interface. These so-called capillary deformations are responsible for capillary interactions between the adsorbed particles [14,15], which regulate the particle self-assembly at the interface [16–18]. These interactions can be tuned by varying, e.g., the particle shape and chemistry [10,19–21], or the curvature of the fluid-fluid interface [22–24]. Very recent experiments [25–27] have shown that adsorbed nanocubes with truncated corners can assemble into graphenelike honeycomb and hexagonal lattices. The origin of these structures is unknown, although ligand adsorption and van der Waals forces between specific facets of the truncated cubes have been suggested [25]. In this Letter, however, we show that generic cubes with homogeneous surface properties generate hexapolar capillary deformations which are largely responsible for the observed structures. Cubes of other materials or dimensions could, therefore, form similar structures.

A primary step for understanding adsorbed-particle systems is the study of an isolated particle at a macroscopically flat fluid-fluid interface. Important issues are the equilibrium configuration of the particle at the interface [28–31] and the adsorption energy [32–34] which depend on the particle shape and chemical properties. A common approximation (following Pieranski [3]) is to assume the fluid-fluid interface to be flat even when the particle is adsorbed, i.e., to ignore the capillary deformations induced by the particle. In this approximation, which is geometrically far from trivial for nonspherical particles, the (free) energy of the particle configuration follows from the particle surface areas below and above the interface plane and from the intersection area of the particle with the interface plane. Numerical techniques employed for these calculations are, e.g., the triangular tessellation technique (TTT) [35–39], and a hit and miss Monte Carlo method [40,41]. However, in this Letter, we will show that neglecting the capillarity can lead to significant overestimates of the energy, and even to erroneous equilibrium configurations of the particle. We calculate the capillary deformations induced by the particle with a new numerical method, recently introduced [42] for 2D systems and here adapted to study 3D adsorbed particles. Our approach differs from Ref. [43], where the linearized Young-Laplace equation is solved, with the location of the triple contact line imposed *a priori* rather than by energy minimization.

First, we briefly illustrate our method. When no particle is adsorbed, the fluid-fluid interface is the flat plane $z = 0$, with area A. Then, we introduce a rigid particle with a fixed position and orientation defined by the polar angle φ of the particle's vertical axis with the interface normal, the internal Euler angle ψ around the particle's vertical axis,

and the height z_c of the particle's center of mass [see Fig. 1(a)]. Possibly, $N > 1$ particles can be introduced, and for each ith particle, the in-plane coordinates x_i and y_i of its center of mass and the azimuthal angle α_i of its vertical axis also need to be specified. The whole particle-fluid-fluid system is surrounded by an external vertical wall at a distance much larger than the particle size. Given fixed volumes of the two fluids, and fixed position(s) and orientation(s) of the particle(s) defined by $\Omega = \{z_{ci}, \varphi_i, \psi_i, x_i, y_i, \alpha_i\}_{i=1}^{N}$, we numerically calculate the fluid-fluid interface equilibrium shape. This is done (see Ref. [42]) by representing the fluid-fluid interface by a grid of points and exploiting a simulated annealing algorithm to calculate the positions of these points that minimize the thermodynamic potential, hereafter called energy, given by [42]

$$E_N(\Omega) = \gamma[S(\Omega) - A + W(\Omega)\cos\theta]. \quad (1)$$

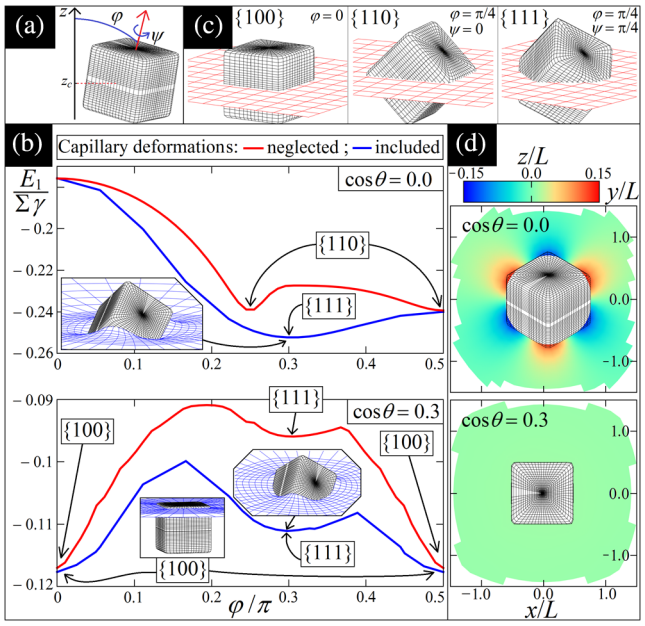

FIG. 1. (a) Configuration of a cubic particle at a fluid-fluid interface. (b) Adsorption energy E_1 [Eq. (1)] of a single cube (side L) at a fluid-fluid interface, in units of $\Sigma\gamma$ (see text), minimized over the center of mass height z_c and the internal Euler angle ψ [see (a)], as a function of the polar angle φ, for Young's contact angle $\cos\theta = 0$ and $\cos\theta = 0.3$. The blue and red lines include and neglect capillarity, respectively. The labels $\{100\}$, $\{110\}$, and $\{111\}$ indicate the cube's orientation in each minimum of the energy. The insets show, for the equilibrium configurations, a 3D view of the interface shape (blue grid) close to the particle (black grid), as calculated by our method. (c) 3D illustration of the $\{100\}$, $\{110\}$, and $\{111\}$ orientations of a cube, where the red grid represents a plane parallel to the flat interface. (d) Contour plots of the deformed-interface height profile for the global minimum-energy configuration of the cube. For $\cos\theta = 0$, a hexapolar deformation emerges, while for $\cos\theta = 0.3$, the interface is essentially undeformed.

Here, $S(\Omega)$ and A are the total area of the fluid-fluid interface with and without particle(s), respectively, and γ is the fluid-fluid surface tension. The total surface area of the particle(s) in contact with the fluid above the interface is $W(\Omega)$, and θ is the Young's contact angle (in the fluid below the interface). Note that γ and θ are input parameters. Equation (1) is defined such that $E_N = 0$ when all the particles are desorbed from the interface into the fluid below. The gravitational energy of the fluid-fluid interface is not included in Eq. (1), as it is negligible when the capillary length ℓ is much larger than the particle size. Also, the particle(s) weight is not included in Eq. (1), as it is typically negligible for sub-mm particles. As proven in Ref. [42], the interface shape that minimizes E_N is the solution of the Young-Laplace equation with Young's Law as boundary condition; i.e., it is the equilibrium shape of the fluid-fluid interface. Note that the position of the three-phase contact line is automatically found by the minimization of E_N; i.e., it is not imposed *a priori*, and the calculated fluid-fluid interface shape forms an angle with the particle surface that matches the input angle θ introduced in Eq. (1).

In this Letter, we show results for cubic particles with smooth edges and side length $L \ll \ell$, where typically $\ell \sim 1$ mm. Since we use a macroscopic fluid-fluid model, we also assume L much larger than the fluid-fluid interface thickness. So our results generally hold for micron-to-nanometer sized cubes. In Fig. 1(b), we show, for a single adsorbed cube, the dependence of E_1, minimized over z_c and ψ, on the polar angle φ, for contact angles given by $\cos\theta = 0$ and $\cos\theta = 0.3$. We plot E_1 in units of $\gamma\Sigma$, with $\Sigma \approx 6L^2$, the cube's total surface area. For a typical surface tension $\gamma = 0.01$ N/m, we have $\Sigma\gamma \approx 350 k_B T$ for $L = 5$ nm, and $\Sigma\gamma \approx 1.5 \times 10^7 k_B T$ for $L = 1$ μm. The coordinates z_c, φ, ψ which locally minimize $E_1(z_c, \varphi, \psi)$ correspond to an equilibrium or metastable configuration of the cube. We found that these are (slight perturbations of) the three configurations shown in Fig. 1(c): $\{100\}$, when one face of the cube points upward; $\{110\}$, when one edge between two faces of the cube points upward; $\{111\}$ when one corner between three faces of the cube points upward. To illustrate the importance of capillarity, we compare, in Fig. 1(b), the energy E_1 with the results obtained from the TTT [44], in which capillarity is neglected. For a given particle configuration, the energy E_1 calculated by the TTT is always higher, as expected. More interestingly, we found that neglecting capillarity leads, for $\cos\theta = 0$, to the wrong equilibrium orientation of the cube: our method predicts $\{111\}$ as equilibrium configuration, whereas the TTT finds $\{110\}$. For $\cos\theta = 0.2$ we find essentially the same equilibrium configuration as for $\cos\theta = 0$ (see Ref. [45]). For $\cos\theta = 0.3$, i.e., for a larger affinity of the cube with the lower fluid, both our numerical method and the TTT predict that $\{100\}$ becomes the minimum-energy configuration, with the cube almost completely immersed

in the lower fluid and without any significant capillarity [see Fig. 1(d)], while $\{111\}$ is now a metastable configuration.

Having established the equilibrium single-cube configuration, we now study the pair interaction and the assembly of many adsorbed cubes. For cubes with $\cos\theta = 0.3$, which induce negligible deformations, we do not expect capillary interactions, in agreement with experiments of cubes with $\cos\theta \approx 0.3$ and $L \approx 1$ μm [46]. Cubes with such a contact angle tend to assemble into tetragonal, possibly closed-packed structures [47]. More interesting is the case $\cos\theta = 0$, where cubes are in the $\{111\}$ configuration and induce a hexapolar deformation in the height profile of the interface, with three depressions and three rises [see Fig. 1(d)]. Similar predictions have also been made for cubes adsorbed at thin films [48]. To study N cubes in such a configuration, we first consider, in Fig. 2(a), the dependence on the particle-particle distance D of the interaction energy per particle

$$\tilde{E}_N \equiv \frac{E_N}{N} - E_1, \tag{2}$$

for $N = 2$, for several relative orientations of the two hexapoles. We indicate a rise induced by a cube in the interface height profile with a red spot, and a depression with a blue spot. Figure 2(a) shows that two cubes attract each other when their orientations allow them to overlap spots with the same color, whereas the cubes repel each other when spots of unlike color overlap. This was to be expected, because the fluid-fluid surface area decreases for overlapping spots of identical color, while it increases when a rise and a depression approach each other. In these calculations, we kept z_c, φ, ψ for each cube fixed to their values for a single-adsorbed cube at $\cos\theta = 0$, as we verified that these are hardly influenced by the presence of the other cubes (see Ref. [49]). To predict the structures in which such cubes assemble, we note from $\tilde{E}_2(D)$ in Fig. 2(a) that there are two kinds of orientations that allow two cubes to attract each other: (i) "dipole-dipole" attraction [Fig. 2(b)], when a set of two spots (one red and one blue) of one cube overlaps with the same set of two spots of another cube, and (ii) a "tripole-tripole" attraction [Fig. 2(c)], when a set of three spots (blue-red-blue or red-blue-red) of one cube overlaps with the same set of three spots of another cube. In Fig. 2(a), we see that the interaction strength $\tilde{E}_2$ for these two different orientations is essentially the same, for $\cos\theta = 0$. However, the contact distance for dipole-dipole interacting cubes is smaller than for tripole-tripole interacting cubes. Therefore, two $\{111\}$-oriented cubes minimize the interaction energy $\tilde{E}_2$ by a dipole-dipole bond, while the tripole-tripole bond is metastable. For $N \gg 2$, dipole-dipole attached cubes can form a hexagonal lattice in which all bonds are satisfied, as shown in Fig. 2(b). Instead, tripole-tripole attached cubes can form a honeycomb lattice with all bonds satisfied, as shown in Fig. 2(c). Note that the holes of this honeycomb lattice are all filled with either depressions or rises, frustrating the inclusion of another $\{111\}$-oriented hexapole-generating cube (see Ref. [50]). In Fig. 2(d), we show, for a periodic extension ($N \to \infty$) of these two lattices, the interaction energy per particle $\tilde{E}_\infty$ [Eq. (2)] as a function of the lattice spacing D. This is calculated by applying our numerical method to a lattice unit cell, which is rectangular with $N = 2$ for the honeycomb lattice and hexagonal with $N = 1$ for the hexagonal lattice. The periodic boundary conditions applied to these unit cells are indicated in Figs. 2(b)–2(d):

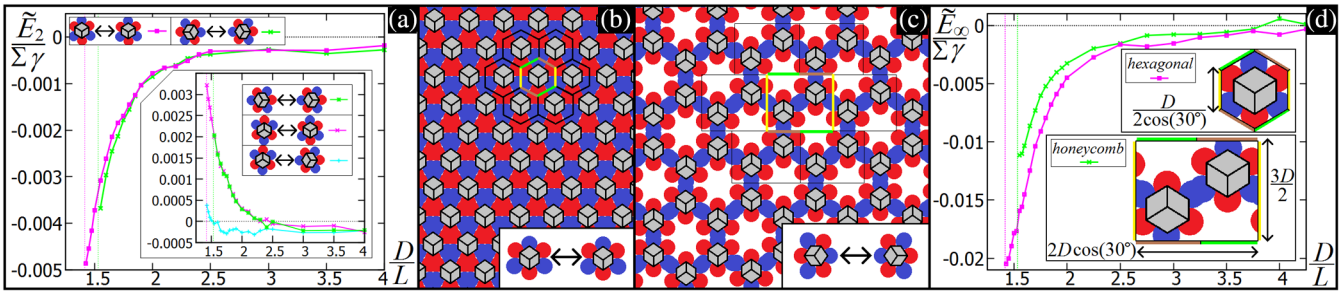

FIG. 2. Results for $\{111\}$-oriented adsorbed cubes with side L and Young's contact angle $\theta = 90°$. (a) Interaction energy per particle $\tilde{E}_2$ [Eq. (2)] of two cubes, in units of $\Sigma\gamma$ (see text), as a function of their center-of-mass distance D, for five relative orientations of their hexapole deformations, sketched in the insets with blue spots for depressions and red spots for rises. The main graph shows the two attractive configurations, where (violet curve) a red-blue dipole approaches another red-blue dipole, and (green curve) a red-blue-red tripole approaches another red-blue-red tripole. The inset shows the two repulsive counterparts and an almost "neutral" dipole-tripole pair. The violet and green vertical dotted lines represent the cube contact distance for the dipole-dipole and tripole-tripole attachments, respectively. As $\cos\theta = 0$, the system is invariant under exchange of red and blue. (b), (c) Sketch of the hexagonal (b) and honeycomb (c) lattices, formed by dipole-dipole and tripole-tripole attached cubes, respectively. Particle-particle distances are only schematic. In the hexagonal lattice, all cubes have the same azimuthal orientation, whereas in the honeycomb, each neighbor is rotated by π. (d) Interaction energy per particle $\tilde{E}_\infty$ [Eq. (2)], as a function of D, for a periodic ($N \to \infty$) hexagonal (violet curve) and honeycomb (green curve) lattice, formed by dipole-dipole and tripole-tripole interacting cubes, respectively. The two insets illustrate the lattice unit cells.

sides of the cell with the same color (yellow, green, and brown) correspond to the same interface height. Contour plots of the interface height profile are shown in Ref. [51], for various lattice spacings. Figure 2(d) shows that, for a given lattice spacing, the hexagonal phase (called phase x) has a lower energy per particle than the honeycomb phase (called phase h). Moreover, phase x can reach a smaller lattice spacing than phase h, and hence, it is tempting to conclude that the equilibrium structure consists of touching cubes in phase x, while the h phase of touching cubes is a metastable state. However, this reasoning on the basis of energetics is only correct if translational and rotational entropy contributions can be ignored, which is only the case in the low-temperature or large-particle regime where $\gamma\Sigma/k_BT$ is sufficiently large. Given the energy scale of about $-0.02\gamma\Sigma$ per particle in the close-packed x phase as shown in Fig. 2(d), and given a typical free-energy scale of $\sim 10k_BT$ per particle in hard disks at packing fractions varying from rather dilute to close-packed, one arrives at a rough estimate of a balance of energetic and entropic contributions for $\gamma\Sigma/k_BT \simeq 500$. This estimate is also borne out by a somewhat more quantitative (albeit still quite approximate) calculation of the free energies per particle of the (x, h, f) phases given by $F_x = \tilde{E}_\infty^{(x)} + F_{hd}^{(x)} - k_BT \ln Z_{\rm or}^{(x)}$, $F_h = \tilde{E}_\infty^{(h)} + F_{hd}^{(f)} - k_BT \ln Z_{\rm or}^{(h)}$, and $F_f = F_{hd}^{(f)}$, respectively, where f labels the disordered fluid phase of $\{111\}$-oriented cubes, $F_{hd}^{(x/f)}$ is the hard-disk free energy in the crystalline or fluid phase for which we use the expressions in Refs. [52,53], and $Z_{\rm or}^{(x/h)} = (3/2\pi)\int_{-\pi/3}^{+\pi/3} d\omega \exp(-C_{x/h}\omega^2/2k_BT)$ is the single-cube orientation partition function. Here, $C_{x/h}$ are spring constants that we extract from our capillary energy calculations by perturbing the relative azimuthal angle ω of neighboring cubes in the x/h phases (see Ref. [54] for details). By performing common tangent constructions of F/A as a function of N/A (see Ref. [55]) to identify coexisting states with different 2D densities $\vartheta^* \equiv N\Sigma/3.24A$, scaled such that $\vartheta^* = 1$ in phase x at close packing, we construct the temperature-density phase diagram in Fig. 3. The blue, green, and purple areas denote one-phase f, h, and x regions, and the gray areas indicate two-phase regions of coexisting phases that can be found by horizontal tie lines. For $\Sigma\gamma/k_BT < 350$ and $\Sigma\gamma/k_BT > 650$, the phase behavior is in the high- and low-temperature limit where the highest-density x phase coexists with the high-density and low-density f phase, respectively. Interestingly, however, in the intermediate regime $350 \lesssim \Sigma\gamma/k_BT \lesssim 650$ that is bounded by an $h-f-x$ and an $f-h-x$ triple point, the h phase is thermodynamically stable in a huge density regime, either coexisting with the f or the x phase, or as a single phase in a tiny density regime. Note that, for such T, cubes are still strongly bound to the interface, as $E_1 \approx -0.25\Sigma\gamma$ for $\theta = 90°$ [see Fig. 1(b)]. To find a stable h phase of cubes with side $L = 5$ nm, a typical tension $\gamma \approx 0.01 - 0.02$ N/m is required at room temperature, which is, indeed, a reasonable estimate for γ in the experiments in Refs. [25,26], where both hexagonal and honeycomb lattices of truncated nanocubes were observed. For cubes with $L = 1$ μm, instead, a much lower tension $\gamma \approx 0.2 - 0.5$ μN/m is needed to obtain the h phase, which could, however, possibly be achieved in the extreme case of, e.g., water-water interfaces [9]. In our analysis, we did not include other kinds of particle-particle interactions, e.g., van der Waals which appear to become relevant only in the limit of nanosized particles at near-contact distances (see Ref. [56]). We leave for future studies the effects of a cubic shape with truncated corners, which could explain the long chain structures at low concentrations observed in Ref. [25].

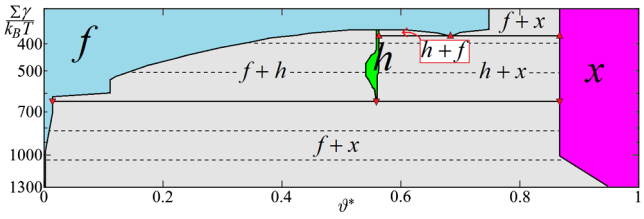

FIG. 3. Temperature-density phase diagram for the adsorbed cubes. In colors, we show the honeycomb-lattice (h), hexagonal-lattice (x), and disordered-fluid (f) phases. The gray area indicates phase coexistence. The normalized density ϑ^* is 1 for the x-phase closest packing density.

In summary, we demonstrate the importance of capillarity for single-cube behavior as well as the self-assembly of many cubes adsorbed at fluid-fluid interfaces. In particular, we showed that cubes with a contact angle close to 90° prefer the $\{111\}$ orientation that generates a hexapolar capillary deformation profile, which leads the cubes to self-assemble into hexagonal and honeycomb lattices. Experiments [60–62] showed that hexagonal platelets self-assemble into honeycomb or hexagonal lattices, depending on whether three or six of the side facets were made hydrophobic. However, here, we theoretically demonstrate that adsorbed cubes with homogeneous surface properties can also self-assemble through capillary interactions into lattices with hexagonal and honeycomb rather than tetragonal symmetries. In addition, with a simple free-energy model, where both configurational entropy and capillary interactions are included, we predict a phase diagram that features both the honeycomb and hexagonal lattices as stable structures. Interestingly, in Refs. [25,26] where hexagonal and honeycomb lattices of adsorbed cubes are actually observed, capillarity is not taken into account to justify such structures, rather ligand adsorption and van der Waals forces between specific facets of the truncated cubes are suggested. Although we cannot exclude other driving forces, our results strongly suggest that capillarity could generate the observed structures. In fact, our phase diagram even features a well-defined parameter

range in which the honeycomb lattice is to be expected, and this region is consistent with the experiments in Refs. [25,26].

The authors acknowledge financial support by a "Nederlandse Organisatie voor Wetenschappelijk Onderzoek" (NWO) Vici Grant and by the Marie Curie Initial Training Network "Soft Matter at Aqueous Interfaces" (SOMATAI). This work is part of the D-ITP consortium, a program of the NWO that is funded by the Dutch Ministry of Education, Culture and Science (OCW).

[1] W. Ramsden, Proc. R. Soc. London **72**, 156 (1903).
[2] S. Pickering, J. Chem. Soc. Trans. **91**, 2001 (1907).
[3] P. Pieranski, Phys. Rev. Lett. **45**, 569 (1980).
[4] S. Sacanna, W. K. Kegel, and A. P. Philipse, Phys. Rev. Lett. **98**, 158301 (2007).
[5] M. G. Basavaraj, S. Vandebril, J. Fransaer, and J. Vermant, Soft Matter **5**, 1717 (2009).
[6] E. Dickinson, Trends Food Sci. Technol. **24**, 4 (2012).
[7] R. Aveyard, Soft Matter **8**, 5233 (2012).
[8] F. Günther, S. Frijters, and J. Harting, Soft Matter **10**, 4977 (2014).
[9] M. Vis *et al.*, ACS Macro Lett. **4**, 965 (2015).
[10] J. Vermant, Nature (London) **476**, 286 (2011).
[11] P. J. Yunker, T. Still, M. A. Lohr, and A. G. Yodh, Nature (London) **476**, 308 (2011).
[12] P. Fang *et al.*, ACS Nano **7**, 9241 (2013).
[13] K. Stratford, R. Adhikari, I. Pagonabarraga, J. C. Desplat, and M. E. Cates, Science **309**, 2198 (2005).
[14] R. Di Leonardo, F. Saglimbeni, and G. Ruocco, Phys. Rev. Lett. **100**, 106103 (2008).
[15] L. Yao, L. Botto, M. Cavallaro, Jr., B. J. Bleier, V. Garbin, and K. J. Stebe, Soft Matter **9**, 779 (2013).
[16] R. McGorty, J. Fung, D. Kaz, and V. N. Manoharan, Mater. Today **13**, 34 (2010).
[17] E. M. Furst, Proc. Natl. Acad. Sci. U.S.A. **108**, 20853 (2011).
[18] A. D. Law, M. Auriol, D. Smith, T. S. Horozov, and D. M. A. Buzza, Phys. Rev. Lett. **110**, 138301 (2013).
[19] A. Kumar, B. J. Park, F. Tu, and D. Lee, Soft Matter **9**, 6604 (2013).
[20] S. Coertjens, P. Moldenaers, J. Vermant, and L. Isa, Langmuir **30**, 4289 (2014).
[21] G. Morris, K. Hadler, and J. Cilliers, Curr. Opin. Colloid Interface Sci. **20**, 98 (2015).
[22] M. Cavallaro, L. Botto, E. P. Lewandowski, M. Wang, and K. J. Stebe, Proc. Natl. Acad. Sci. U.S.A. **108**, 20923 (2011).
[23] C. Blanc, D. Fedorenko, M. Gross, M. In, M. Abkarian, M. A. Gharbi, J. B. Fournier, P. Galatola, and M. Nobili, Phys. Rev. Lett. **111**, 058302 (2013).
[24] D. Ershov, J. Sprakel, J. Appel, M. A. Cohen Stuart, and J. van der Gucht, Proc. Natl. Acad. Sci. U.S.A. **110**, 9220 (2013).
[25] W. H. Evers, B. Goris, S. Bals, M. Casavola, J. de Graaf, R. van Roij, M. Dijkstra, and D. Vanmaekelbergh, Nano Lett. **13**, 2317 (2013).
[26] M. P. Boneschanscher *et al.*, Science **344**, 1377 (2014).
[27] W. Beugeling, E. Kalesaki, C. Delerue, Y.-M. Niquet, D. Vanmaekelbergh, and C. Morais Smith, Nat. Commun. **6**, 6316 (2015).
[28] G. Morris, S. J. Neethling, and J. J. Cilliers, Minerals engineering **33**, 87 (2012).
[29] B. J. Park, C.-H. Choi, S.-M. Kang, K. E. Tettey, C.-S. Lee, and D. Lee, Langmuir **29**, 1841 (2013).
[30] L. Isa, N. Samudrala, and E. R. Dufresne, Langmuir **30**, 5057 (2014).
[31] E. L. Sharp, H. Al-Shehri, T. S. Horozov, S. D. Stoyanov, and V. N. Paunov, RSC Adv. **4**, 2205 (2014).
[32] K. Du, E. Glogowski, T. Emrick, T. P. Russell, and A. D. Dinsmore, Langmuir **26**, 12518 (2010).
[33] L. Isa, E. Amstad, K. Schwenke, E. Del Gado, P. Ilg, M. Kröger, and E. Reimhult, Soft Matter **7**, 7663 (2011).
[34] G. B. Davies, T. Krueger, P. V. Coveney, and J. Harting, J. Chem. Phys. **141**, 154902 (2014).
[35] J. de Graaf, M. Dijkstra, and R. van Roij, J. Chem. Phys. **132**, 164902 (2010).
[36] A. R. Morgan, N. Ballard, L. A. Rochford, G. Nurumbetov, T. S. Skelhon, and S. A. F. Bon, Soft Matter **9**, 487 (2013).
[37] W. van der Stam, A. P. Gantapara, Q. A. Akkerman, G. Soligno, J. D. Meeldijk, R. van Roij, M. Dijkstra, and C. de Mello Donega, Nano Lett. **14**, 1032 (2014).
[38] B. Peng, G. Soligno, M. Kamp, B. de Nijs, J. de Graaf, M. Dijkstra, R. van Roij, A. van Blaaderen, and A. Imhof, Soft Matter **10**, 9644 (2014).
[39] N. Ballard and S. A. F. Bon, J. Colloid Interface Sci. **448**, 533 (2015).
[40] B. J. Park and D. Lee, Soft Matter **8**, 7690 (2012).
[41] B. J. Park and D. Lee, ACS Nano **6**, 782 (2012).
[42] G. Soligno, M. Dijkstra, and R. van Roij, J. Chem. Phys. **141**, 244702 (2014).
[43] K. D. Danov, P. A. Kralchevsky, B. N. Naydenov, and G. Brenn, J. Colloid Interface Sci. **287**, 121 (2005).
[44] J. de Graaf, M. Dijkstra, and R. van Roij, Phys. Rev. E **80**, 051405 (2009).
[45] See Supplemental Material, Fig. S1 at http://link.aps.org/supplemental/10.1103/PhysRevLett.116.258001 for the energy of a single-adsorbed cube with $\cos\theta = 0.2$ and $\cos\theta = 0.5$.
[46] J. W. J. de Folter, E. M. Hutter, S. I. R. Castillo, K. E. Klop, A. P. Philipse, and W. K. Kegel, Langmuir **30**, 955 (2014).
[47] M. Pang, A. J. Cairns, Yu. Liu, Y. Belmabkhout, H. C. Zeng, and M. Eddaoudi, J. Am. Chem. Soc. **135**, 10234 (2013).
[48] G. Morris, S. Neethling, and J. Cilliers, J. Colloid Interface Sci. **361**, 370 (2011).
[49] See Supplemental Material, Fig. S2 at http://link.aps.org/supplemental/10.1103/PhysRevLett.116.258001 for the energy of two adsorbed and interacting cubes, with respect to their single-cube configuration.
[50] See Supplemental Material, Fig. S3 at http://link.aps.org/supplemental/10.1103/PhysRevLett.116.258001 for the energy of six and seven tripole-tripole interacting cubes in a honeycomb and hexagonal arrangement, respectively.
[51] See Supplemental Material, Fig. S4 at http://link.aps.org/supplemental/10.1103/PhysRevLett.116.258001 for contour plots of the interface height profile in the honeycomb and hexagonal lattices, for several lattice spacings.
[52] Y. Rosenfeld, Phys. Rev. A **42**, 5978 (1990).

[53] D. A. Young and B. J. Alder, J. Chem. Phys. **70**, 473 (1979).
[54] See Supplemental Material, Sec. IV at http://link.aps.org/supplemental/10.1103/PhysRevLett.116.258001 for the free-energy model used to predict the phase diagram in Fig. 3.
[55] See Supplemental Material, Fig. S9 at http://link.aps.org/supplemental/10.1103/PhysRevLett.116.258001 for plots of the free energy for the hexagonal-lattice, honeycomb-lattice and disordered-fluid phases, at various values of T.
[56] See Supplemental Material, Secs. V and VI at http://link.aps.org/supplemental/10.1103/PhysRevLett.116.258001 for an order-of-magnitude estimation of van der Waals and Casimir-like forces in typical experimental systems, which includes Refs. [58–60].
[57] P. C. Hiemenz and R. Rajagopalan, *Principles of Colloid and Surface Chemistry*, 3rd ed. (Marcel Dekker, Inc., New York, 1997).
[58] D. V. Talapin and E. V. Shevchenko, Nano Lett. **7**, 1213 (2007).
[59] M. Oettel, A. Domínguez, and S. Dietrich, Phys. Rev. E **71**, 051401 (2005).
[60] N. Bowden, A. Terfort, J. Carbeck, and G. M. Whitesides, Science **276**, 233 (1997).
[61] N. Bowden, I. S. Choi, B. A. Grzybowski, and G. M. Whitesides, J. Am. Chem. Soc. **121**, 5373 (1999).
[62] D. B. Wolfe, A. Snead, C. Mao, N. B. Bowden, and G. M. Whitesides, Langmuir **19**, 2206 (2003).